J Mater Sci (2016) 51:9761–9770

Electronic structure, ferroelectric properties, and phase stability of $BiGaO_3$ under high pressure from first principles

J. Kaczkowski[1,*]

[1] *Institute of Molecular Physics Polish Academy of Sciences, ul. M. Smoluchowskiego 17, 60-179 Poznan, Poland*

Received: 5 May 2016
Accepted: 9 July 2016
Published online: 18 July 2016

ABSTRACT

High-pressure behavior of $BiGaO_3$ has been investigated from 0 to 20 GPa using density functional theory. It is found that $BiGaO_3$ undergoes a pressure-induced first-order phase transition from pyroxene (Pcca) to monoclinic (Cm) at 3.5 GPa, and then to rhombohedral (R3c) at 5.2 GPa, and finally to orthorhombic (Pnma) structure at 7.4 GPa. The first phase transition (Pcca → Cm) agrees well with the experimental results. At 5.2 GPa the possible coexistence of three ferroelectric phases, i.e., monoclinic Cm, tetragonal P4mm, and rhombohedral R3c has been predicted. The calculated values of spontaneous polarization for these phases are of 124.87, 123.48, 88.75 μC/cm^2 for Cm, P4mm, and R3c, respectively.

Introduction

In recent years, the Bi-based perovskites have attracted an increasing interest as a less-toxic alternative to the most widely used ferroelectric material, lead zirconate titanate [1, 2]. The stereochemically active $6s^2$ lone pair on the Pb^{2+} or Bi^{3+} ions is responsible for the large ion off-centering in Pb- and Bi-based perovskites and, as a result, the large ferroelectric polarization. Among bismuth perovskite oxides, $BiGaO_3$ has been studied extensively since the first theoretical report [3], in which large ferroelectric polarization was predicted with the value of 151.9 μC/cm^2 for tetragonal ground-state structure (space group P4mm). A high-pressure and high-temperature technique was used to prepare $BiGaO_3$ samples [4]. Experimental results have shown that $BiGaO_3$ crystallizes in the pyroxene structure (space group Pcca). A modified sol–gel method was used to synthesize nanocrystalline $BiGaO_3$ films with orthorhombic structure [5]. The ellipsometric measurements have shown that $BiGaO_3$ is indirect band gap oxide with the value of the gap 2.17 eV, which made it suitable for photovoltaic devices [5]. Further experimental investigation revealed that perovskite-like structures appear under chemical or hydrostatic pressure. The coexistence of polar rhombohedral (space group R3c) and monoclinic (space group Cm) phases was observed in solid solution $BiFe_{1-x}Ga_xO_3$ at $x = 0.1$ [6] and $x = 0.2$–0.4 [7] and $BiCr_{1-x}Ga_xO_3$ at $x = 0.8$ [7]. For these solid solutions large values of spontaneous polarization were predicted using the point charge model, i.e., 58 μC/cm^2 for $BiGa_{0.4}Cr_{0.6}O_3$, 116 μC/cm^2 for $BiGa_{0.4}Fe_{0.6}O_3$, and 102 μC/cm^2

Address correspondence to E-mail: kaczkowski@ifmpan.poznan.pl

DOI 10.1007/s10853-016-0211-2

$BiGa_{0.7}Mn_{0.3}O_3$ [7]. The supertetragonal-like structure was observed in $BiFe_{0.6}Ga_{0.4}O_3$ thin films [8]. The giant ferroelectric polarization of 230 $\mu C/cm^2$ for $BiGa_{1-x}Fe_xO_3$ [6] and 150 $\mu C/cm^2$ for $BiFe_{0.6}Ga_{0.4}O_3$ [8] was found. The nonpolar orthorhombic (space groups Imma and Pnma) and monoclinic (space group C2/c) phases were observed in bulk $BiCr_{1-x}Ga_xO_3$ [7, 9] and $BiMn_{1-x}Ga_xO_3$ [7]. In the first report on structural behavior of $BiGaO_3$ as a function of pressure, Yusa et al. [10] showed that it undergoes three pressure-induced phase transitions in the 0–11 GPa range, from pyroxene structure (Pcca space group) to the perovskite-like monoclinic Cm phase, and then to the orthorhombic Cmcm, and finally from Cmcm to Pbam structure at 3.2, 6.3, and 9.8 GPa, respectively.

From the theoretical side, the pyroxene phase of $BiGaO_3$ has been characterized by density functional calculations. The majority of reports is focused on the structural, electronic, and vibrational properties of the pyroxene phase of $BiGaO_3$ at ambient conditions [5, 11–13]. There are also several studies of the perovskite cubic phase of $BiGaO_3$ [14–17]. But to our knowledge, there are no theoretical reports concerning pressure-induced structural phase transitions for $BiGaO_3$. Study of high-pressure phases could shed light on physical properties of phases which appear in different solid solutions of $BiGaO_3$ systems [6–9, 18–20]. In addition, in other perovskites, hydrostatic pressure may cause similar effects to chemical doping [21, 22]. For example, it has been shown that the rhombohedral to orthorhombic phase transition in $BiFeO_3$ can be caused by rare-earth doping [21] or hydrostatic pressure [22]. In this paper we investigate structural, electronic, and ferroelectric properties of different crystallographic phases of $BiGaO_3$ under high pressure.

This paper is organized as follows: in the next section the description of the method of calculations is presented, further we present results and discussion, and finally short summation is given.

Method of calculations

The calculations were done using the density functional theory (DFT) within the projector augmented wave (PAW) method [23, 24] as implemented in Vienna ab initio Simulation Package (VASP) [25]. The pseudopotentials used in our calculations were taken from the VASP pseudopotential library [24]. The d-states were treated as core states for Bi and as valence states for Ga. We considered the following space groups: Pcca, Cm, Cmcm, Pbam, R3c, Pnma, C2/c, and Imma. These space groups have been reported in the experimental studies on $BiGaO_3$ under hydrostatic or chemical pressure [4–7, 9, 10]. In addition, we have also investigated five space groups: Pm-3m, P4mm, R3m, C2/m, and R-3c, which have not been observed in experiment but were investigated theoretically in the Ref. [3]. Experimentally established structural data from Refs. [7, 10] were used as input for the calculations. The Brillouin zone integrations were performed using $12 \times 12 \times 12$, $8 \times 8 \times 8$, $8 \times 8 \times 8$, and $6 \times 6 \times 6$ Gamma-centered k-point grids for cell with 5- (Pm-3m, P4mm, R3m), 10- (C2/m, Cm, R3c, R-3c), 20- (C2/c, Cmcm, Imma, Pcca, Pnma), and 40-atoms (Pbam), respectively. A kinetic energy cutoff 520 eV and a total energy convergence threshold of 10^{-6} eV were used. The Brillouin zone sampling was checked to render converged results. The increasing number of *k*-points has small effect on phase energy differences. The cell shape and internal atomic positions were optimized within GGA with the Perdew–Burke–Ernzerhof (GGA-PBE) functional [26] and local density approximation (LDA) [27]. All results presented in this work were done within GGA-PBE until otherwise stated. All aforementioned structures were relaxed by minimizing their enthalpy at a series of pressures between 0 and 20 GPa.

Results

First, we compare the total energies of fully optimized aforementioned phases of $BiGaO_3$ at ambient pressure within both generalized gradient and local density approximations. The results are presented in Table 1. From the total energy calculations within GGA-PBE the pyroxene Pcca phase is the most stable. The same calculations within LDA give the lowest energy for the perovskite monoclinic Cm phase. Only the GGA-PBE correctly predicts the pyroxene phase to be the crystallographic ground state of $BiGaO_3$, while the LDA fails to do so. In Ref. [28] similar calculations have been performed for P4mm, R3c, R-3c, and R3m phases of $BiGaO_3$ within LDA. The calculated total energy differences relative to P4mm were 0.041, 0.185, and 0.234 eV for R3c, R3m, and

Table 1 Computed energy differences (meV/f.u.) between different structural phases of $BiGaO_3$ at ambient pressure relative to the pyroxene Pcca phase

Phase	E-E(Pcca) [meV/f.u.]	
	GGA	LDA
Cm	9	−8
C2/m	112	70
C2/c	33	3
Pcca	0	0
Pbam	34	5
Pnma	32	1
Cmcm	47	13
Imma	45	12
P4mm	12	−7
R3 m	38	13
R3c	23	−4
R-3c	51	16
Pm-3m	112	70

R-3c, respectively. The same values in our case are 0.038, 0.202, and 0.236 eV. This result is in a good agreement with those presented in Ref. [28]. Other phases presented here were not considered in Ref. [28].

In order to study the energetic stability of the selected phases of $BiGaO_3$ under high pressure, we plotted the pressure-relative enthalpy (P-ΔH) curves for each phase relative to pyroxene Pcca phase, as shown in Fig. 1. For the considered phases, the minimum enthalpy path is Pcca → Cm → R3c → Pnma. These phase transitions occur at 3.5, 5.2, and 7.4 GPa, respectively. The theoretical prediction of the first phase transition from pyroxene Pcca to perovskite monoclinic Cm phase agrees well with the experimental findings reported in Ref. [10]. The calculated transition pressure of 3.5 GPa is in good agreement with the experimental result of 3.2 GPa from Ref. [10]. For higher values of pressure there is no such agreement. The first disagreement is that the theoretical values of transition pressure are lower than the experimental ones. The second disagreement is that R3c and Pnma phases were not observed in the experiment [10].

There are several possible explanations of these discrepancies. First, it could be connected with the existence of high energy barriers not included in our calculations. Such situation has been observed in $LiNbO_3$ [29]. Another source of difference between experiment and theory could arise from the

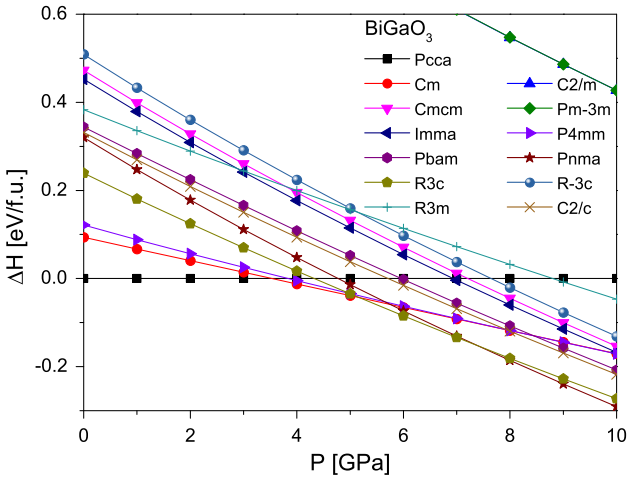

Figure 1 Relative enthalpies (meV/f.u.) between pyroxene Pcca phase and the other space groups as a function of pressure.

difficulties in measurements i.e., nonhydrostatic conditions, quality of samples, etc. For example, the high-pressure phase diagram of $BiFeO_3$ or $PbZr_{1-x}Ti_xO_3$ is still unclear despite numerous experimental and theoretical studies [30–33]. In case of $BiGaO_3$, there is only one experimental report so far [10]. We believe that future experiments will give more decisive answer about the symmetry of high-pressure phases of $BiGaO_3$.

The calculated volumes of Pcca, Cm, R3c, and Pnma phases as a function of pressure are shown in Fig. 2. There is a 6.6 % volume collapse at 3.5 GPa during the phase transition from Pcca pyroxene to Cm perovskite. This value is in a good agreement with the experimental measurement from Ref. [10]

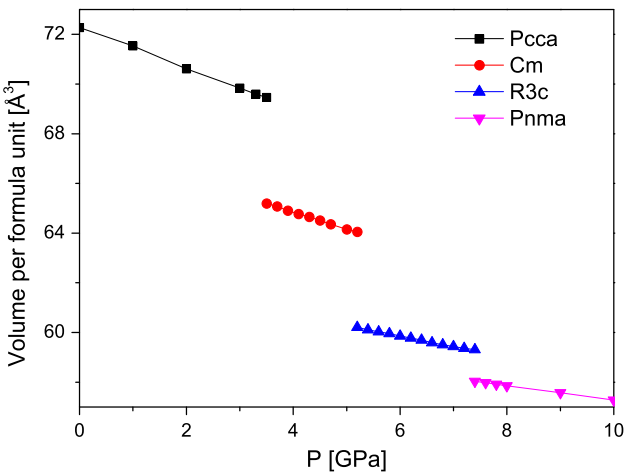

Figure 2 Volume of the unit cell (per f.u.) for the most stable structures of $BiGaO_3$ as a function of pressure.

which is 6.5 %. Despite the disagreement in predicting crystal structure in the second phase transition, the calculated volume changes is similar to the experimental ones in Ref. [10]. For the theoretically predicted phase transition from the monoclinic Cm to the rhombohedral R3c there is a 6 % volume change at 5.2 GPa. The volume change measured in experiment at 6.3 GPa during the phase transition from the monoclinic Cm to the orthorhombic Cmcm is 5 %. The value of volume change for another phase transition in Ref. [10] (i.e., from Cmcm to Pbam) is not given, but from pressure–volume plot (Fig. 9 in the Ref. [10]) we see, that it is smaller than other ones. In our case, the value of calculated volume change from the rhombohedral R3c to the orthorhombic Pnma is 2 %, which is also smaller than in the earlier phase transitions.

Our data show that around 5 GPa there is a possibility of coexistence of three polar phases, i.e., monoclinic Cm, tetragonal P4mm, and rhombohedral R3c. This situation could be similar to the one in $PbZr_{1-x}Ti_xO_3$ [30, 31]. The calculated structural parameters of these phases at the transition pressures are given in Table 2. In general, the values of these parameters are slightly overestimated and deviate from experimental results by less than 2 %. Only the

Table 2 Calculated lattice parameters and ionic positions of the pyroxene Pcca, monoclinic Cm, rhombohedral R3c, and orthorhombic Pnma phase of $BiGaO_3$ at ambient and transition pressures

Phase	Reference	Pressure (GPa)	Lattice parameters	Wyckoff positions
Pcca	GGA-PBE this work	0.0	$a = 5.503$ Å; $b = 5.195$ Å; $c = 10.112$ Å	Bi(4d): 0.25, 0, 0.6091 Ga(4e): 0.25, 0.5, 0.3557 O1(4c): 0, 0.6471, 0.25 O2(8f): 0.9041, 0.2324, 0.0546
Pcca	Experiment ref. [4]	0.0	$a = 5.416$ Å; $b = 5.134$ Å; $c = 9.937$ Å	Bi(4d):0.25, 0, 0.6098 Ga(4e):0.25, 0.5, 0.3583 O1(4c):0, 0.6333, 0.25 O2(8f):0.9055, 0.2314, 0.0503
Pcca	Experiment ref. [5]	0.0	$a = 5.626$ Å; $b = 5.081$ Å; $c = 10.339$ Å	–
Cm	GGA-PBE this work	0.0	$a = 5.293$ Å; $b = 5.259$ Å; $c = 4.876$ Å; $\beta = 92.99^{o}$	Bi(2a):0, 0, 0; Ga(2a):0.4545, 0, 0.5624; O(2a):0.4289, 0, 0.1847; O(4b):0.2049, 0.2480, 0.7056
Cm	GGA-PBE this work	3.5	$a = 5.244$ Å; $b = 5.224$ Å; $c = 4.763$ Å; $\beta = 92.20^{o}$	Bi(2a):0, 0, 0; Ga(2a):0.4558, 0, 0.5631; O(2a):0.4346, 0, 0.1778; O(4b):0.2056, 0.2489, 0.7053
Cm	Experiment ref. [10]	3.2	$A = 5.217$ Å; $b = 5.210$ Å; $c = 4.570$ Å; $\beta = 91.35°$	–
R3c	GGA-PBE this work	0.0	$a = 5.660$ Å; $\alpha = 59.16^{o}$	Bi(2a):0, 0, 0; Ga(2):0.2212, 0.2212, 0.2212; O(6b):0.2837, 0.6906, 0.8245
R3c	GGA-PBE this work	5.2	$a = 5.557$ Å; $\alpha = 59.67°$	Bi(2a):0, 0, 0; Ga(2):0.2256, 0.2256, 0.2256; O(6b):0.2817, 0.6881, 0.8243
Pnma	GGA-PBE this work	0.0	$a = 5.676$ Å; $b = 7.814$ Å; $c = 5.461$ Å	Bi(4c):0.0537, 0.25, 0.9908; Ga(4b):0, 0, 0.5; O(4c):0.9736, 0.25, 0.4091; O(8d):0.2012, 0.9562, 0.1980
Pnma	GGA-PBE this work	7.4	$a = 5.581$ Å; $b = 7.712$ Å; $c = 5.394$ Å	Bi(4c):0.0513, 0.25, 0.9907; Ga(4b):0, 0, 0.5; O(4c):0.9772, 0.25, 0.4124; O(8d):0.2030, 0.9575, 0.1992

value of the c constant in the monoclinic Cm phase is overestimated by 4 %. However, in all cases this overestimation is less than 5 % which is typical for GGA-PBE functional. The tetragonal P4mm phase has a large tetragonality ($c/a = 1.286$), which is in good agreement with the previous theoretical report ($c/a = 1.30$) [3]. The effective tetragonality in monoclinic Cm phase is given by $2\sqrt{2}c/(a + b)$. The calculated value of this parameter at 5.2 GPa is 1.279. The large value of effective tetragonality of Cm phase is in good agreement with the experimental results for solid solutions of $BiGa_{0.4}Fe_{0.6}O_3$ and $BiGa_{0.7}Mn_{0.3}O_3$ (both 1.25) from Ref. [7]. For the phases with very large c/a ratio, the large spontaneous polarization is expected. The value of spontaneous polarization is defined by:

$$P_\alpha = \frac{e}{\Omega}\sum_{\kappa,\beta} Z_{\kappa,\alpha\beta}\delta_{\kappa,\beta},$$

where P_α is the spontaneous polarization in the α direction, Ω is the volume of the unit cell, $Z_{\kappa,\alpha\beta}$ is the $\alpha\beta$ element of the Born effective charge tensor of the atom κ, $\delta_{\kappa,\beta}$ is the displacement of atom κ along the β direction from the centrosymmetric position. The centrosymmetric reference structures were R-3c for R3c, C2/m for Cm, and P4/mmm for P4mm. The Born effective charge (BEC) tensors were calculated by density functional perturbation theory as implemented in VASP [34]. The same approach has been used in our previous works on ferroelectric properties of $BiFeO_3$ [35] and $BiAlO_3$ [36]. In Table 3 we only present these values at 5.2 GPa. For other pressures these values do not deviate very much. The nominal ionic values of Bi, Ga, and O are +3, +3, and −2.

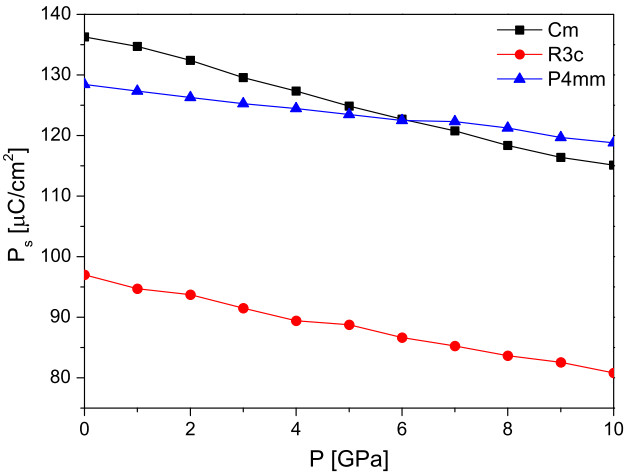

Figure 3 Polarization magnitude as a function of pressure for the monoclinic Cm, tetragonal P4mm, and rhombohedral R3c phase of $BiGaO_3$.

Table 3 Calculated Born effective charge tensors and the high-frequency static dielectric tensor (ε_∞) for the monoclinic Cm, tetragonal P4mm, and rhombohedral R3c phase of $BiGaO_3$

Atom	xx	yy	zz	xy	xz	yx	yz	zx	zy
Cm									
Bi	5.37	5.27	3.02	0.00	0.29	0.00	0.00	0.33	0.00
Ga	2.98	2.98	3.57	0.00	0.14	0.00	0.00	0.01	0.00
O1	−2.86	−2.80	−2.43	0.00	−0.26	0.00	0.00	−0.33	0.00
O2	−2.74	−2.73	−2.08	0.23	−0.09	0.24	−0.10	−0.01	−0.03
ε_∞	6.07	6.14	4.87	0.00	0.20	0.00	0.00	0.20	0.00
P4mm									
Bi	5.51	5.51	2.98	0.00	0.00	0.00	0.00	0.00	0.00
Ga	2.94	2.94	3.59	0.00	0.00	0.00	0.00	0.00	0.00
O1	−2.92	−2.92	−2.39	0.00	0.00	0.00	0.00	0.00	0.00
O2	−3.05	−2.48	−2.08	0.00	0.00	0.00	0.00	0.00	0.00
O3	−2.48	−3.05	−2.08	0.00	0.00	0.00	0.00	0.00	0.00
ε_∞	6.27	6.27	4.88	0.00	0.00	0.00	0.00	0.00	0.00
R3c									
Bi	4.60	4.82	4.87	−0.09	−0.31	−0.30	0.26	0.06	−0.43
Ga	3.32	3.38	3.42	−0.03	−0.10	−0.14	0.12	0.06	−0.21
O1	−3.00	−2.28	−2.84	0.43	−0.19	0.33	0.45	−0.22	0.23
O2	−2.76	−2.80	−2.58	−0.25	0.50	−0.19	0.22	0.67	0.04
O3	−2.16	−3.12	−2.87	0.21	−0.30	0.03	−0.30	−0.13	−0.41
ε_∞	6.01	6.19	6.23	−0.15	−0.10	−0.15	−0.06	−0.10	−0.06

The BEC tensors of $BiGaO_3$ in the monoclinic Cm and tetragonal P4mm structures are diagonal (P4mm) or almost diagonal (Cm), which indicate that the spontaneous polarization should be along the axial direction. The xx and yy components of the BEC tensors of Bi and O are anomalously large with respect to their nominal ionic values, while the zz component is almost equal to them. The values of the BEC tensor of Ga are almost close to the nominal ionic value. The BEC tensors of $BiGaO_3$ in the rhombohedral R3c phase have nonzero values in the off-diagonal components. The diagonal elements in x and y directions of these tensors in case of Bi and O atoms are larger than their nominal ionic charges but smaller than in case of Cm and P4mm phases. This is connected to the large c/a ratio in monoclinic and tetragonal phases. The larger distance between the bismuth and the surrounding oxygen weakens hybridization (the calculated values of Bi-O length are 3.86, 3.80, and 3.28 Å for Cm, P4mm, and R3c phase, respectively). Similar behavior has been observed in $BiFeO_3$ [28]. The high values of the BEC tensors in perovskite oxides indicate the presence of ferroelectricity [37]. In Fig. 3 the calculated spontaneous polarization as a function of pressure for three polar phases is presented. In Table 4 the calculated values of spontaneous polarization at 0 and 5.2 GPa for Cm, P4mm, and R3c phases are given. At ambient pressure the magnitudes of spontaneous polarization are 136.26, 128.44, 97.01 $\mu C/cm^2$ for Cm, P4mm, and R3c phase, respectively. The direction of spontaneous

Table 4 Calculated values of spontaneous polarization of three polar phases of $BiGaO_3$ at 0 GPa and 5.2 GPa pressures

	0 GPa	5.2 GPa
Cm	136.26	124.87
P4mm	128.44	123.48
R3c	97.01	88.75

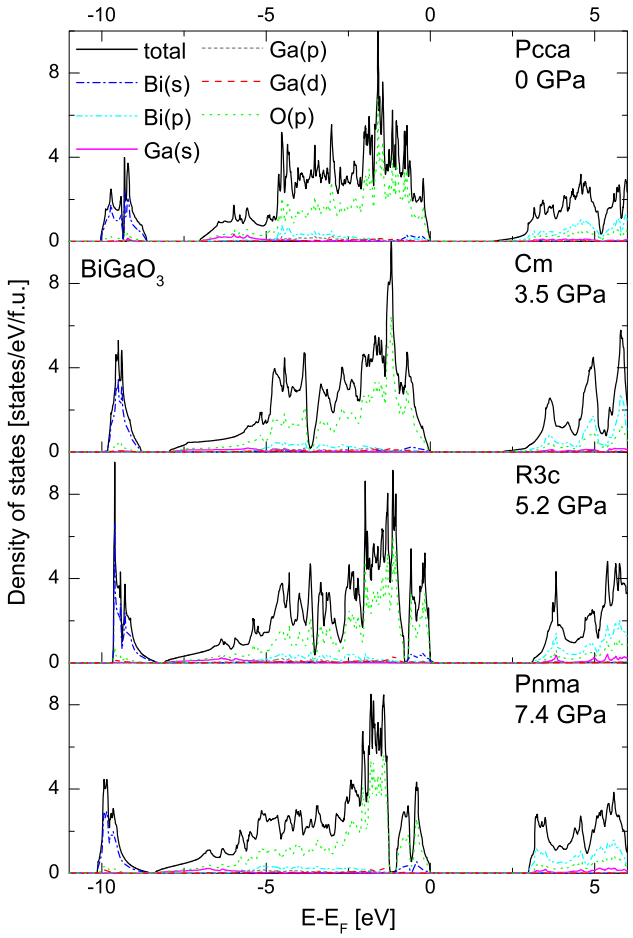

Figure 4 The total and partial density of states of four different phases of $BiGaO_3$ at their transition pressures.

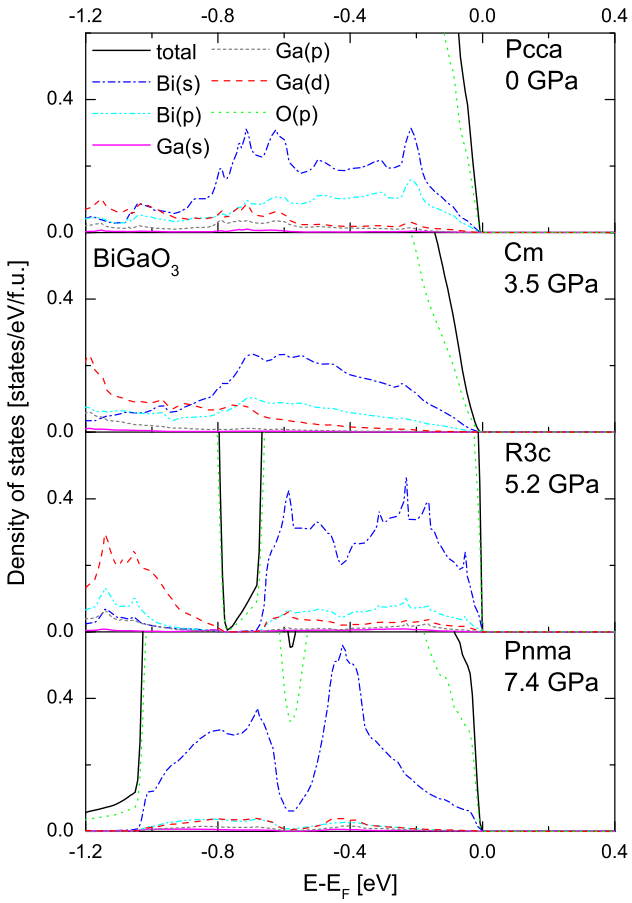

Figure 5 The total and partial density of states near the Fermi level.

polarization is along [111] in R3c phase and it is along [001] in P4mm phase. For Cm phase the values of polarization are 44.86, 0, 124.83 μC/cm^2 along x, y, and z directions, respectively. Despite the fact that the presence of these phases at 0 GPa is hypothetical, it is worth noticing that for the rhombohedral R3c phase the value of polarization is larger than that of $BiFeO_3$ (90.9 μC/cm^2) [35] and $BiAlO_3$ (81 μC/cm^2) [36] (both crystallize in R3c at ambient conditions) from our previous work. At the region of possible phase coexistence, i.e., at 5.2 GPa, these values are 124.87, 123.48, 88.75 μC/cm^2 for Cm, P4mm, and R3c phase, respectively. For P4mm the value of 152 μC/cm^2 has been predicted in the Ref. [3]. The coexistence of phases with large difference between spontaneous polarizations along different directions is important from technological point of view because it makes it possible to switch between these phases using an electric field [38]. Such phase coexistence could be obtained by the chemical pressure instead of the hydrostatic pressure. So far, the aforementioned phase coexistence of the monoclinic Cm and the rhombohedral R3c phases of $BiGaO_3$ has been observed in solid solutions with Fe [6, 7] and Cr [7].

The ferroelectric properties of aforementioned phases are caused by stereochemically active 6s^2 lone pairs on bismuth ions. To show this the electronic structure calculations were performed and the results are given in Figs. 4, 5, 6. In Fig. 4 we present the total and partial density of states for four phases at their theoretically predicted transition pressures. The detailed studies of the electronic structure of the Pcca pyroxene phase at ambient pressure were given elsewhere [13]. In general, in all phases the valence

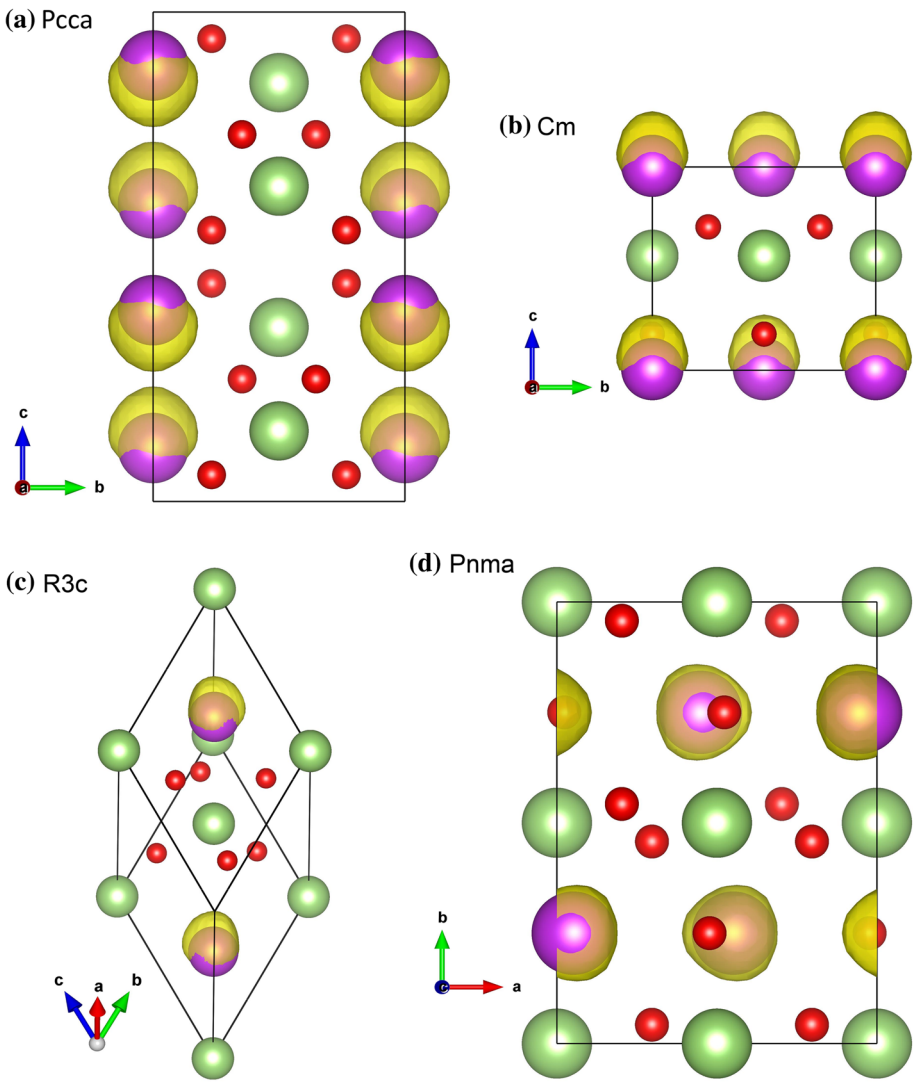

Figure 6 Electron localization function (ELF) of the most stable phases of $BiGaO_3$ at the value of 0.9. The figure was generated using the VESTA visualization package [42].

band (VB) is split into two separate subbands. The upper part of the VB (from 0 to 8 eV below the Fermi level) consists mainly of the O-2p states with small contribution from the Ga-3sp states and the Bi-6sp states. Below these bands the Bi-6s states appear with small contributions from O-2p states. The conduction band (CB) is characterized by empty Bi-6p and O-2p states with small contribution from Ga-3s states. The occupied Bi-6s and O-2p states form the bonding (8–10 eV below the Fermi level) and antibonding (near the Fermi level, Fig. 5) states, respectively. In case of centrosymmetric Pcca pyroxene, noncentrosymmetric Cm and R3c perovskites the antibonding states hybridize with Bi-6p states (see Fig. 5) which lead to the asymmetric electron distribution around the Bi atoms. There is no such hybridization in case of centrosymmetric Pnma perovskite. The situation for Pcca, Cm, and R3c is typical in the formation of lone pairs [39]. This can be visualized with the help of the electron localization function (ELF) which is shown in Fig. 6. ELF is a tool for analysis of the character of the chemical bond [40, 41] and is a measure of the probability of finding an electron near another same-spin electron. The values of ELF are between 0 and 1. The high values of ELF describes region where there is no chance to find two same-spin electrons and is interpreted as a presence of the lone pairs. In our case the ELFs are localized near the Bi atoms in all aforementioned phases. However, the ELFs are strongly asymmetric in the case of Pcca, Cm, and R3c, and symmetric in the case of Pnma. In case of Pcca pyroxene the lone pairs are arranged in opposite manner due to the centrosymmetric structure. For monoclinic Cm and rhombohedral R3c the lone pairs promote structural distorsion and, as a result, these phases are ferroelectric.

Conclusions

The ground-state properties as well as high-pressure behavior of $BiGaO_3$ were studied by means of the first-principles method. We have found the following sequence of phase transitions: Pcca → Cm → R3c → Pnma, which occur at 3.5, 5.2, and 7.4 GPa, respectively. Only the first phase transition (Pcca → Cm) has been observed experimentally. At 5.2 GPa the coexistence of three ferroelectric phases i.e., monoclinic Cm, tetragonal P4mm, and rhombohedral R3c has been predicted with the high values of spontaneous polarization of 124.87, 123.48, 88.75 μC/cm^2, respectively. For these structures the mixing of Bi-s, Bi-p, and O-p states near the top of the valence band is responsible for the formation of the lone pair in the vicinity of the bismuth atoms and, as a result, for ferroelectric properties. In addition, the large values of the spontaneous polarization in case of Cm and P4mm phases are caused by large tetragonality (∼1.3).

Acknowledgements

This work was supported by the National Science Centre (Poland) through the Grant No. DEC-2011/01/B/ST3/02212.

References

[1] Panda PK (2009) Review: environmental friendly lead-free piezoelectric materials. J Mater Sci 44:5049–5062. doi:10.1007/s10853-009-3643-0

[2] Belik AA (2012) Polar and nonpolar phases of $BiMO_3$: a review. J Solid State Chem 195:32–40

[3] Baettig P, Schelle ChF, LeSar R, Waghmare UV, Spaldin NA (2005) Theoretical prediction of new high-performance lead-free piezoelectrics. Chem Mater 17:1376–1380

[4] Belik AA, Wuernischa T, Kamiyama T, Mori K, Maie M, Nagai T, Matsui Y, Takayama-Muromachi E (2006) High-pressure synthesis, crystal structures, and properties of perovskite-like $BiAlO_3$ and pyroxene-like $BiGaO_3$. Chem Mater 18:133–139

[5] Zhang JZ, Ding HC, Zhu JJ, Li YW, Hu ZG, Duan CG, Meng XJ, Chu JH (2014) Electronic structure and optical responses of nanocrystalline $BiGaO_3$ films: a combination study of experiment and theory. J Appl Phys 115:083110-1–083110-5

[6] Yan J, Gomi M, Yokota T, Song H (2013) Phase transition and huge ferroelectric polarization observed in $BiFe_{1-x}Ga_xO_3$ thin films. Appl Phys Lett 102:222906-1–222906-4

[7] Belik AA, Rusakov DA, Furubayashi T, Takayama-Muromachi E (2012) $BiGaO_3$-based perovskites: a large family of polar materials. Chem Mater 24:3056–3064

[8] Fan Z, Xiao J, Liu H, Yang P, Ke Q, Ji W, Yao K, Ong KP, Zeng K, Wang J (2015) Stable ferroelectric perovskite structure with giant axial ratio and polarization in epitaxial $BiFe_{0.6}Ga_{0.4}O_3$ thin films. ACS Appl Mater Interfaces 7:2648–2653

[9] Belik AA (2015) Magnetic properties of solid solutions between $BiCrO_3$ and $BiGaO_3$ with perovskite structures. Sci Technol Adv Mater 16:026003-1–026003-8

[10] Yusa H, Belik AA, Takayama-Muromachi E, Hirao N, Ohishi Y (2009) High-pressure phase transitions in $BiMO_3$ (M=Al, Ga, and In): in situ x-ray diffraction and Raman scattering experiments. Phys Rev B 80:214103-1–214103-10

[11] Li C, Wang B, Wang R, Wang H, Lu X (2008) First-principles study of structural, elastic, electronic, and optical properties of orthorhombic $BiGaO_3$. Comput Mater Sci 42:614–618

[12] Sai G, Yue-Hue W, Xin-Yin Z, Min Z, Na Z, Yi-Feng D (2011) Structural, electronic, and optical properties of $BiAl_xGa_{1-x}O_3$ (x = 0, 0.25, 0.5, and 0.75). Chin Phys Lett 28:087402-1–087402-4

[13] Kaczkowski J (2014) Electronic structure and lattice dynamics of orthorhombic $BiGaO_3$. J Alloys Compd 613:175–180

[14] Wang H, Wang B, Li Q, Zhu Z, Wang R, Woo CH (2007) First-principles study of the cubic perovskites $BiMO_3$ (M=Al, Ga, In, and Sc). Phys Rev B 75:245209-1–245209-9

[15] Wang H, Wang B, Wang R, Li Q (2007) Ab initio study of structural and electronic properties of $BiAlO_3$ and $BiGaO_3$. Phys B 390:96–100

[16] Kaczkowski J, Jezierski A (2013) Electronic structure of the cubic perovskites $BiMO_3$ (M=Al, Ga, In, Sc). Acta Phys Pol, A 124:852–854

[17] Behram RB, Iqbal MA, Alay-E-Abbas SM, Sajjad M, Yaseen M, Arshad MI, Murtaza G (2016) Theoretical investigation of mechanical, optoelectronic, and thermoelectric properties of $BiGaO_3$ and $BiInO_3$ compounds. Mater Sci Semicond Process 41:297–303

[18] Cheng JR, Zhu W, Li N, Cross LE (2003) Fabrication and characterization of $xBiGaO_3$-$(1-x)PbTiO_3$: a high temperature reduced Pb-content piezoelectric ceramic. Mater Lett 57:2090–2094

[19] Zhou C, Liu X, Li W, Yuan C, Chen G (2010) Structure and electrical properties of Bi0.5(Na, K)0.5TiO3-BiGaO3 lead-free piezoelectric ceramics. Curr Appl Phys 10:93–98

[20] Xing J, Tan Z, Yuan J, Jiang L, Chen Q, Wu J, Zhang W, Xiao D, Zhu J (2016) Structure and electrical properties of $(0.965-x)(K_{0.48}Na_{0.52})NbO_3$-$xBiGaO_3$-$0.035(Bi_{0.5}Na_{0.5})ZrO_3$ piezoelectric ceramics. RSC Adv 6:57210–57216

[21] Kan D, Pálová L, Anbusathaian V, Cheng CJ, Fujino S, Nagarajan V, Rabe KM, Takeuchi I (2010) Universal behavior and electric-field-induced structural transition in rare-earth-substituted $BiFeO_3$. Adv Funct Mater 20:1108–1115

[22] Guennou M, Bouvier P, Chen GS, Dkhil B, Haumont R, Garbarino G, Kreisel J (2011) Multiple high-pressure phase transitions in $BiFeO_3$. Phys Rev B 84:174107-1–174107-10

[23] Blöchl PE (1994) Projector augmented-wave method. Phys Rev B 50:17853–17979

[24] Kresse G, Joubert D (1999) From ultrasoft pseudopotentials to the projector augmented-wave method. Phys Rev B 59:1758–1775

[25] Kresse G, Furthmüller J (1996) Efficient iterative schemes for ab initio total-energy calculations using a plane-wave basis set. Phys Rev B 54:11169–11186

[26] Perdew JP, Burke K, Ernzerhof M (1996) Generalized gradient approximation made simple. Phys Rev Lett 77:3865–3868

[27] Perdew JP, Zunger A (1981) Self-interaction correction to density-functional approximations for many-electron systems. Phys Rev B 23:5048–5079

[28] Okuno Y, Sakashita Y (2009) Born effective charges and piezoelectric coefficients of $BiXO_3$. Jpn J Appl Phys 48:09KF04-1–09KF04-4

[29] Nakamura K, Higuchi S, Ohnuma T (2012) First-principles investigation of pressure-induced phase transition in $LiNbO_3$. J Appl Phys 111:033522-1–033522-6

[30] Noheda B, Cox DE, Shirane G, Gonzalo JA, Cross LE, Park S-E (1999) A monoclinic ferroelectric phase in $Pb(Zr_{1-x}Ti_x)O_3$ solid solution. Appl Phys Lett 74:2059–2061

[31] Yokota H, Zhang N, Taylor AE, Thomas PA, Glazer AM (2009) Crystal structure of the rhombohedral phase of $PbZr_{1-x}Ti_xO_3$ ceramics at room temperature. Phys Rev B 80:104109-1–104109-12

[32] Kornev IA, Bellaiche L, Janolin P-E, Dkhil B, Suard E (2006) Phase diagram of Pb(Zr, Ti)O3 solid solution from first principles. Phys Rev Lett 97:157601-1–157601-4

[33] Catalan G, Scott JF (2009) Physics and applications of bismuth ferrite. Adv Mater 21:2463–2485

[34] Gajdoš M, Hummer K, Kresse G, Furthüller J, Bechstedt F (2006) Linear optical properties in the projector-augmented wave methodology. Phys Rev B 73:045112-1–045112-9

[35] Pugaczowa-Michalska M, Kaczkowski J (2015) First-principles study of structural, electronic, and ferroelectric properties of rare-earth-doped $BiFeO_3$. J Mater Sci 50:6227–6235. doi:10.1007/s10853-015-9183-x

[36] Kaczkowski J (2016) Electronic structure and lattice dynamics of rhombohedral $BiAlO_3$ from first-principles. Mater Chem Phys. doi:10.1016/j.matchemphys.2016.04.045

[37] Zhong W, King-Smith RD, Vanderbilt D (1994) Giant LO-TO splittings in perovskite ferroelectrics. Phys Rev Lett 72:3618–3621

[38] Diéguez O, Íñiguez J (2011) First-principles investigation of morphotropic transitions and phase-change functional responses in $BiFeO_3$-$BiCoO_3$ multiferroic solid solutions. Phys Rev Lett 107:057601-1–057601-5

[39] Walsh A, Payne DJ, Egdell RG, Watson GW (2011) Stereochemistry of post-transition metal oxides: revision of the classical lone pair model. Chem Soc Rev 40:4455–4463

[40] Becke AD, Edgecombe KE (1990) A simple measure of electron localization in atomic and molecular systems. J Phys Chem 92:5397–5403

[41] Silvi B, Savin A (1994) Classification of chemical bonds based on topological analysis of electron localization functions. Nature 371:683–686

[42] Momma K, Izumi F (2011) VESTA 3 for three-dimensional visualization of crystal, volumetric and morphology data. J Appl Crystallogr 44:1272–1276